**Astronomy
&
Astrophysics**

Excitation and damping of slow magnetosonic standing waves in a solar coronal loop

M. Selwa[1], K. Murawski[1], and S. K. Solanki[2]

[1] Institute of Physics, UMCS, ul. Radziszewskiego 10, 20-031 Lublin, Poland
   e-mail: mselwa@kft.umcs.lublin.pl
[2] Max-Planck-Institut für Sonnensystemforschung, Max-Planck-Str. 2, 37191 Katlenburg-Lindau, Germany

Abstract. We consider slow magnetosonic standing waves that are impulsively excited in a solar coronal loop. The one-dimensional numerical model we implement includes the effects of nonlinearity, optionally thermal conduction, heating, and cooling of the solar plasma. We numerically evaluate excitation and damping times of a standing wave in hot coronal loops on the basis of a parametric study. Results of the numerical simulations reveal that initially launched impulses mainly trigger the fundamental mode and its first harmonic, depending on the location of these pulses in space. Parametric study shows that these standing waves are excited in a dozen or so wave periods corresponding roughly to 13 min and that they are strongly damped over a similar time-scale.

Key words. Sun: corona – Sun: magnetohydrodynamics (MHD) – Sun: oscillations

1. Introduction

Coronal loop oscillations have recently become a subject of considerable observational and theoretical interest. Impulsively generated, standing slow waves in hot ($T > 6$ MK) loops have been detected with SOHO/SUMER (Wang et al. 2003a). It is interesting that these standing waves are strongly attenuated while the loops cool down (Curdt et al. 2003). Observations from the SUMER and EIT on SOHO and TRACE have revealed that Yohkoh loop oscillations often seem to be triggered by micro- or sub-flares near a loop foot-point (Wang et al. 2003b). In such cases the trigger may be plasma flow injected into the loop from one foot-point.

Several attenuation mechanisms have been proposed: wave leakage into the chromosphere (Ofman 2002; Van Doorsselaere et al. 2004), lateral wave leakage due to curvature of loops (Roberts 2000), phase mixing (Nakariakov 1999; Ofman & Aschwanden 2002), resonant absorption (Ruderman & Roberts 2002), and non-ideal MHD effects (Roberts 2000). In particular, Ofman & Wang (2002) have found that thermal conduction leads to rapid damping of slow standing waves, with a less significant contribution from compressive viscosity (Ofman et al. 2002a). Ofman et al. (2002b) have shown that a nonlinear steepening of slow waves leads to their enhanced dissipation. Nakariakov et al. (2000a) have found that dissipation and stratification are the main factors influencing slow wave evolution, while De Moortel et al. (2002a) have deduced that thermal conduction can account for the observed damping times.

In another study, Nakariakov et al. (2004) and Tsiklauri et al. (2004) demonstrated that in a coronal loop an impulsive energy release efficiently excites the second spatial harmonic. The considered model included the effects of gravitational stratification, heat conduction, radiative losses, external heat input, and Braginskii bulk viscosity. An extensive review of longitudinal intensity fluctuations observed in coronal loops is presented by De Moortel et al. (2002b).

Our work is aimed at an explanation of the excitation mechanism of slow standing waves, while including main damping mechanism, i.e. thermal conduction. We discuss impulsively generated waves that are described by fully nonlinear one-dimensional ideal MHD equations. As a consequence of this one-dimensional assumption, the Alfvén and fast magnetosonic waves are removed from the physical system, which only contains the slow waves.

2. A numerical model

As we only pay attention to slow waves, we consider that the coronal loop lies along the x-direction. Additionally we assume that velocity $\boldsymbol{V} = [V, 0, 0]$, magnetic field $\boldsymbol{B} = [B, 0, 0]$, and the plasma quantities only depend on time t and coordinate x. As a consequence of these assumptions we adopt the one-dimensional MHD equations:

$$\frac{\partial \varrho}{\partial t} + \frac{\partial (\varrho V)}{\partial x} = 0, \tag{1}$$

$$\varrho \left(\frac{\partial V}{\partial t} + V \frac{\partial V}{\partial x} \right) = -\frac{\partial p_{\mathrm{T}}}{\partial x}, \tag{2}$$

$$\frac{\partial (\varrho E)}{\partial t} + \frac{\partial [(\varrho E + p_{\mathrm{T}})V]}{\partial x} = \frac{\partial}{\partial x} \left(\sigma \frac{\partial T}{\partial x} \right) + \mathcal{H} - \mathcal{L}, \tag{3}$$

$$\frac{\partial B}{\partial t} = \frac{\partial B}{\partial x} = 0. \tag{4}$$

Here ϱ is the mass density, T – the temperature, and the symbol p_T denotes a total pressure that represents the sum of the gas and magnetic pressures:

$$p_T = \left(p + \frac{B^2}{2\mu} \right), \tag{5}$$

where μ is the magnetic permeability. E is the plasma energy density:

$$E = \frac{\varrho V^2}{2} + \frac{p_T}{\gamma - 1}, \tag{6}$$

where γ is the adiabatic index. Coefficient σ corresponds to the thermal conductivity that follows from the formulation of Spitzer (1962)

$$\sigma = \kappa T^{5/2}, \tag{7}$$

where $\kappa = 9.2 \times 10^{-7}$ erg cm^{-1} s^{-1} K$^{-7/2}$ is the plasma thermal conductivity.

In Eq. (3) $\mathcal{L}$ represents a cooling term due to radiative losses from an optically thin plasma (Raymond 1978) and $\mathcal{H}$ is the heating term that is implemented phenomenologically as (Zingale et al. 2002)

$$\mathcal{H} = \mathcal{H}_0 \exp\left[-\frac{(x - x_0)^2}{2w_h^2} \right] \exp\left(-\frac{t}{\tau} \right). \tag{8}$$

We choose and fix the width of the heating source $w_h = 1.25 \times 10^8$ cm, $\mathcal{H}_0 = 0.2$ erg cm^{-3} s^{-1}, the duration $\tau = 41$ s, while the spatial position of heat deposition x_0 is left as a free parameter. These values correspond to parameters of a typical solar flare according to Nakariakov et al. (2004).

2.1. The loop equilibrium

We consider the equilibrium at which pressure $p_0 = c_s^2 \varrho_0/\gamma =$ const. and plasma is at rest, $V_0 = 0$. We choose equilibrium density profile ϱ_0, which varies with x such that ϱ_0 attains large values at loop foot-points settled at $x = 0$ and $x = L$, where $L = 50 \times 10^8$ cm is the loop length which corresponds to loop radius of $13-16$ Mm. The loop is relatively short because short loops are easier to simulate. In Sect. 3.2 we also consider loops with other lengths. The mass density profile $\varrho_0(x)$ is similar to the profile implemented by Ofman (2002), i.e.

$$\varrho_0(x) = \varrho_c \left\{ \frac{d}{2} \left[\tanh \left(s \left(x - x_{tr} \right) \cdot \left(x - L + x_{tr} \right) \right) + 1 \right] + 1 \right\}. \tag{9}$$

Here d is the ratio of the photospheric mass density ϱ_{ph} to coronal mass density $\varrho_c = 10^{-15}$ g cm^{-3}. We allow this parameter to vary in the range $10^4 \leq d \leq 10^8$. The quantity $s = 0.5 \times 10^{-17}$ cm^{-1} denotes the slope of $\varrho_0(x)$ at the loop foot-points, and $x_{tr} = 0.2842 \times 10^8$ cm corresponds to the position of the transition region. According to Eq. (9) ϱ_0 jumps at this location. As $T_0(x) \sim p_0/\varrho_0(x)$, the plasma temperature T_0 is higher at the solar corona than at the foot-points. We also choose the sound speed in the solar corona $c_s = \sqrt{\gamma p_0/\varrho_0(x = L/2)} = 0.35 \times 10^8$ cm s^{-1}.

2.2. Perturbations

For the coronal loop that is described by Eqs. (1)–(3), perturbations can be excited in such a loop in numerous ways. Here we focus our attention on impulsively excited waves. We launch a hot pulse in the mass density, pressure, and velocity. This pulse has the following form:

$$\delta\varrho(x, t = 0) = A_\varrho \exp\left[-(x - x_0)^2/w^2 \right], \tag{10}$$

$$\delta p(x, t = 0) = A_p \exp\left[-(x - x_0)^2/w^2 \right], \tag{11}$$

$$\delta V(x, t = 0) = A_V \exp\left[-(x - x_0)^2/w^2 \right], \tag{12}$$

where A_ϱ, A_p, and A_V are initial amplitudes of the pulse, x_0 its initial position, and w its initial width.

2.3. Analytical formulae for standing waves

To derive analytical formulae for standing waves, we replace the profile of Eq. (9) by a uniform profile $\varrho_0 = $ const., then neglect thermal conduction, heating, and cooling by setting $\sigma = \mathcal{H} = \mathcal{L} = 0$ in Eq. (3). Additionally we assume solid-wall boundary conditions at $x = 0$ and $x = L$ by setting $V = 0$ there. In this case initial perturbations after a sufficiently long time excite the standing wave oscillations given by the analytical formulae:

$$V(x, t) = A_v \cos(\omega_n t) \sin(k_n x), \tag{13}$$

$$\delta\varrho(x, t) = -\frac{\varrho_0 A_v}{c_s} \sin(\omega_n t) \cos(k_n x), \tag{14}$$

$$\delta p(x, t) = -\varrho_0 A_v c_s \sin(\omega_n t) \cos(k_n x), \tag{15}$$

where:

$$k_n = \frac{n\pi}{L}, \qquad \omega_n = c_s k_n. \tag{16}$$

Notice that perturbed mass density $\delta\varrho$ and velocity V display a phase shift of a quarter wave period.

3. Numerical results

In this part of the paper we present numerically obtained results for various run parameters. The plasma equations are solved numerically with the FLASH code (Fryxell et al. 2000). For most numerical runs 300 blocks are chosen. Each block contains 8 grid cells. We performed grid convergence studies to verify that the numerical diffusion is negligibly small. Free boundary conditions are used at the boundaries of the simulation region, and all physical quantities are measured in cgs units.

We discuss the fundamental mode and the first harmonic, which are both triggered by temperature perturbations and go on to pay particular attention to excitation and damping times of these modes. Our simulations show that these lowest modes are the dominantly excited ones for the pulse parameters employed.

3.1. Excitation by temperature perturbation

We now consider the case of ideal plasma for which there is no thermal conduction, cooling, and heating. This implies that
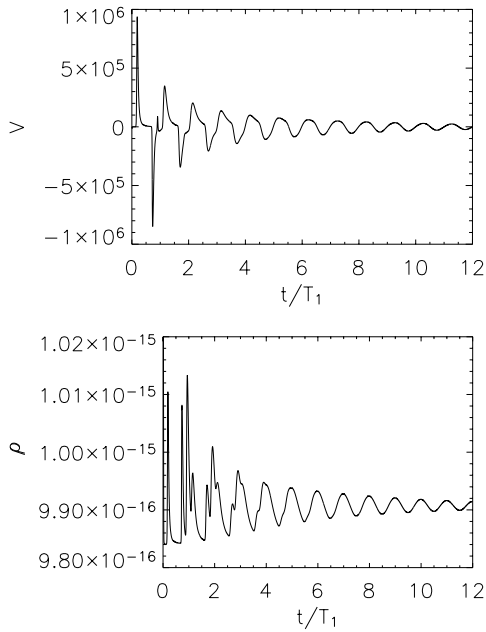
Fig. 1. Evolution of velocity $V(x = L/4, t)$ (*top panel*) and mass density $\varrho(x = L/4, t)$ (*bottom panel*) for mass density contrast $d = 10^8$, pulse width $w = L/40$, and initial pulse position $x_0 = L/4$.
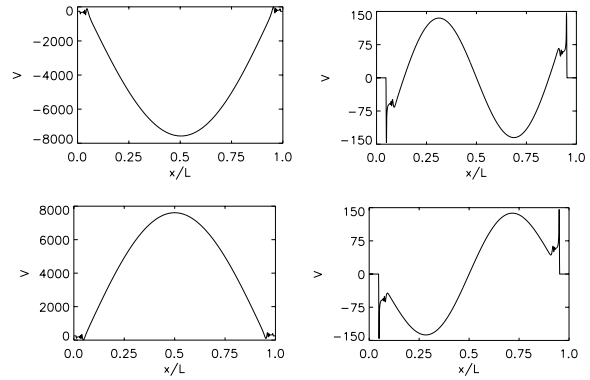

Fig. 2. Spatial profiles of velocity $V(x, t = 18.842\ T_1)$ (*left top panel*), $V(x, t = 19.274\ T_1)$ (*left bottom panel*), $V(x, t = 37.841\ T_2)$ (*right top panel*), and $V(x, t = 38.281\ T_2)$ (*right bottom panel*) for mass density contrast $d = 10^8$, pulse width $w = L/40$, pulse position $x_0 = L/4$ (*left panels*), and $x_0 = L/2$ (*right panels*). Left (*right*) profiles correspond to the fundamental (first harmonic) mode.
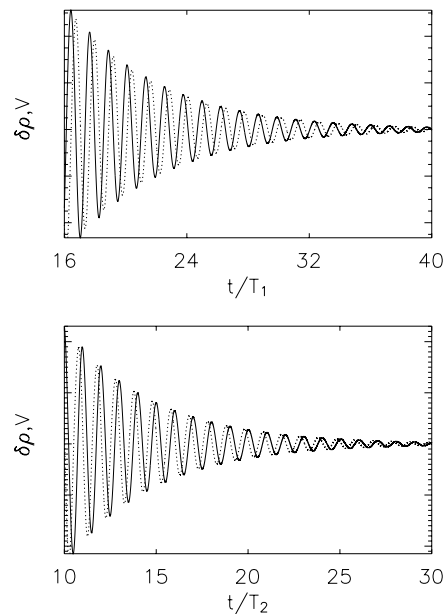
Fig. 3. Time-signatures of perturbed mass density $\delta\varrho(x = L/4, t)$ (solid line) and velocity $V(x = L/4, t)$ (dashed line) for $d = 10^8$, $w = L/40$, $x_0 = L/4$ (*top panel*), and $x_0 = L/2$ (*bottom panel*).

the source terms on the right hand side of Eq. (3) are set to zero. So, we have $\sigma = \mathcal{L} = \mathcal{H} = 0$. Additionally we assume that there are no initial velocity perturbations. In this case slow waves are excited solely by temperature perturbations given by Eqs. (10)–(12) with $A_\varrho = 0.125\,\varrho_0(x_0)$, $A_p = 0.25\,p_0$, and $A_V = 0$. We launch the pulses of Eqs. (10)–(11) with a width of $w = L/40$, which is a typical value determined from observations (Nakariakov et al. 2004). We also carry out a parametric study in which parameters are allowed to vary around the adopted fiducial values. First we consider in some detail three cases that correspond to different positions of the initial pulses: (a) $x_0 = L/4$; (b) $x_0 = L/2$; (c) $x_0 = 0$.

3.1.1. Time evolution of the pulses

The basic time-signature of the excited mode is similar to a damped oscillation (see Fig. 1). However, the wave form evolves significantly with time. At the initial stages of evolution and in addition to the signal that is typical of standing mode, we observe some short-wave oscillations (Fig. 1), also seen in FFT spectra – not shown – and in wavelet spectra (Fig. 4). At later times the signal becomes almost sinusoidal.

3.1.2. Pulses at a quarter of the loop length and at the apex of the loop

If the initial pulse is launched at $x_0 = L/4$ ($x_0 = L/2$), the fundamental (first harmonic) mode is excited. Figure 2 displays spatial profiles of these waves at given moments in time. As the fundamental standing wave is twice longer than its harmonic (Fig. 2), the fundamental wave is less sensitive to the inhomogeneous medium, and essentially it occupies the cavity over all its length L. The harmonic wave is more sensitive to the

inhomogeneity than the fundamental wave, resulting in enhanced energy leakage into the photosphere.

Time-signatures of perturbed mass density $\delta\varrho$ and velocity V, which are detected at spatial point $x = L/4$, are shown in Fig. 3 for a time after the initial high frequency power has died away. Oscillation amplitudes decrease with time as a consequence of wave damping due to energy leakage into the photosphere.

In all considered cases the presence of the standing wave in the system is evaluated on the basis of normalized phase shift $\delta\phi$, for the fundamental ($n = 1$) or harmonic ($n = 2$) standing waves. We establish *an excitation criterion* according to which a standing wave is present in the system if $\delta\phi$ departs
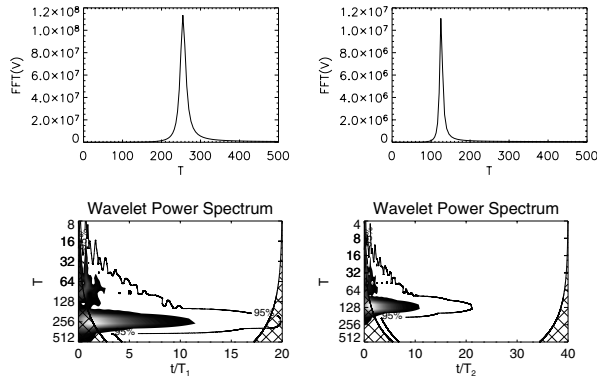
Fig. 4. Spectra of velocity $V(x = L/4, t)$ from Fig. 3. The Fourier spectra are displayed in the top panels and the corresponding wavelet spectra in the bottom panels. Both the Fourier and wavelet analysis lead to wave periods $T_1 \approx 254$ s, $T_2 \approx 125$ s, where T_n is the nth standing wave period. The hatched area in the lower frames indicate regions where the wavelet transform is less accurate.

by 20% from 1/4, since the quarter period lag is a signature of the analytical solution of Sect. 2.3 , viz.

$$\frac{1}{4} \cdot 80\% \leq \delta\phi \leq \frac{1}{4} \cdot 120\%. \tag{17}$$

This criterion is fulfilled for $t > t_{\min}$. As the standing wave excitation time we assume $t_{\min}$. According to this criterion the fundamental (harmonic) standing wave is excited at $t \approx 6\,T_1$ ($t \approx 3.5T_2$), where T_1 and T_2 are the analytically evaluated periods that are expressed by

$$T_n = \frac{2L_{\mathrm{eff}}}{nc_s}, \tag{18}$$

where n denotes the standing wave number, c_s – the sound speed, and L_{eff} – the effective loop length. From Fig. 2 we estimate that $L_{\mathrm{eff}} \approx 45 \times 10^8$ cm and then $T_1 \approx 257$ s and $T_2 \approx 128$ s. These values are close to the results of the fast Fourier transform (FFT) and wavelet analyses (Fig. 4). Small differences result from the fact that the effective length of the cavity is lower than L and differs for the case of $n = 1$ and $n = 2$. Moreover, c_s is an inhomogeneous function of x in our simulations, but is assumed to be x-independent when evaluating Eq. (18).

We have restricted the Fourier analysis to $t > 3\,T_1$ in order to remove the transient signal at the initial stage of temporal evolution. This signal is discernible in the wavelet power spectrum (Fig. 4) obtained using a Morlet mother function (Torrence & Compo 1998)

$$\psi(\eta) = \pi^{-1/4} e^{im\eta} e^{-\eta^2/2}$$

with $m = 6$. The wavelet transform was applied to the full time series. The solid contour represents 95% confidence, and the shaded area 90%.

3.1.3. A pulse at a foot-point

The initial pulse of Eqs. (10)–(11) is launched at the loop foot-point located at $x = 0$. Figure 5 displays the corresponding
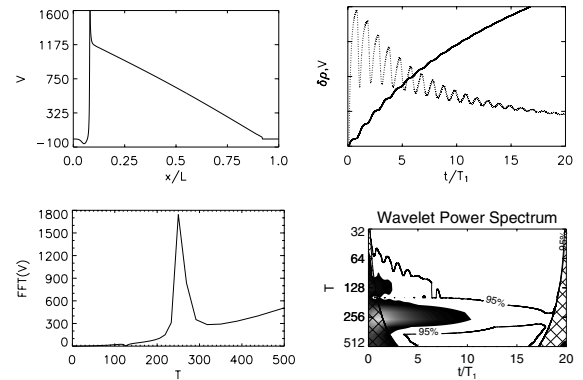
Fig. 5. A spatial velocity profile at $t \approx 20\,T_1$ (*left top panel*), time-signatures (*right top panel*) of the perturbed mass density $\delta\varrho(x = L/4, t)$ (solid line), and velocity $V(x = L/4, t)$ (dotted line) for $d = 10^8$, $w = L/40$, and $x_0 = 0$. The corresponding Fourier and wavelet power spectra are displayed in the bottom panels.

results. As a result of a hot initial pulse, plasma is heated locally at the loop foot-point. Just warmed-up and dense photospheric plasma leaves the excitation region and fills up the coronal loop. As a consequence, $\delta\varrho$ grows in time (top right panels). The mean flow is directed to the loop center, and its efficiency declines both spatially in the region $x > x_0$ (left top panel) and with time (right top panel). Velocity power spectra (bottom panels) reveal the wave period of the fundamental standing wave T_1. The background in the Fourier power spectrum is introduced by the velocity drift. The wave excitation time $t_{\mathrm{ex}} \approx 3\,T_1$, and the damping time $\tau \approx 5\,T_1$. Qualitatively similar results have been obtained in the case of the initial pulse launched in the photosphere at $x_0 = -L/50$, i.e. outside the loop, corresponding to subsurface layers of the Sun (not shown). Recently Tsiklauri et al. (2004) discussed the case of heat deposition at a loop-foot point.

3.1.4. Excitation of a packet of standing waves

We excite different waves by setting the initial pulses in different parts of the loop. Fourier spectra show that an almost pure first harmonic standing wave is excited when the initial pulse is launched at the loop apex. In some cases we do not observe a single standing mode but instead a packet of modes in which the fundamental and harmonic standing modes make the largest contribution. Moving the excitation point from the loop apex to the foot-points results in an excitation of the fundamental mode. For the excitation points that are close to $x_0 = L/2$ we observe that the Fourier power in the first harmonic standing mode is much higher than in the fundamental standing mode, while for $x_0 = 3L/8$ the scenario changes and the fundamental mode dominates (Fig. 6).

3.2. Parametric studies of wave excitation and damping times

In this part of the paper we present results of parametric studies. We vary several parameters, such as pulse position x_0, density contrast d, pulse width w, temperature of initial pulses, and
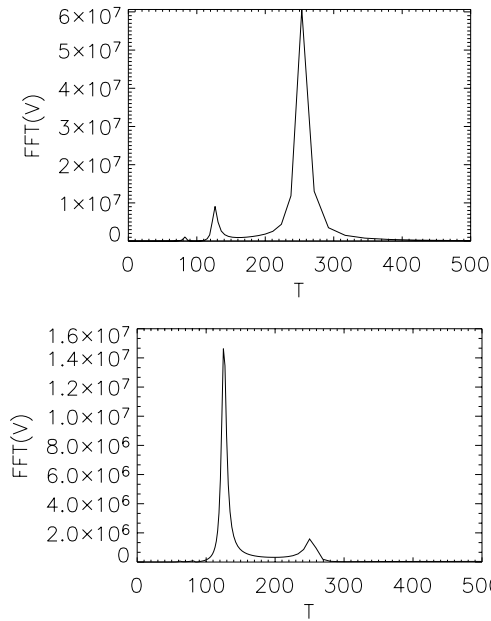
Fig. 6. Fourier spectra of the velocity $V(x = L/4, t)$ for $d = 10^8$, $w = L/40$, $x_0 = 0.375L$ (*top panel*), and $x_0 = 0.475L$ (*bottom panel*). Fundamental and the first harmonic standing modes are dominant in the top and bottom panels, respectively, but the first harmonic and fundamental modes are present there too.

Fig. 7. Normalized standing wave excitation time t_{ex}/T_n (*top panel*) and normalized damping time τ/T_n (*bottom panel*) vs. normalized pulse position x_0/L for $d = 10^8$ and $w = L/40$. The squares (crosses) correspond to the fundamental (harmonic) standing waves.

perturbations in velocity A_V. We analyze how the standing wave excitation time t_{ex} and damping time τ depend on these parameters.
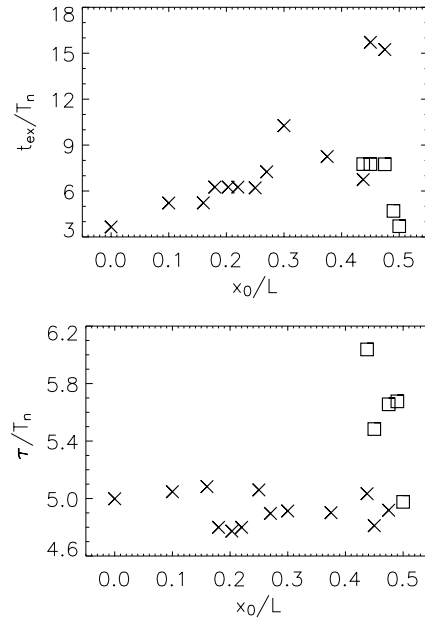
We first filter out non-oscillatory components from the time-signatures $\varrho(x_0 = L/4, t)$ and $V(x_0 = L/4, t)$ to remove trends, such as seen in the upper right panel of Fig. 5, and to get a pure signal that corresponds solely to oscillations. The filtering is done by the code originally developed by Ofman (2002). We estimate excitation time t_{ex} with the criterion described by Eq. (17), while for damping time τ we fit an envelope of a velocity profile into the following formula

$$V(x = x_d, t) = V_0 \exp\left(-\frac{t - t_{ex}}{\tau}\right), \quad t \geq t_{min}, \tag{19}$$

where x_d denotes the detection point, and V_0 is the amplitude of the velocity V at time t_{ex}.

We first consider the dependence of t_{ex} and τ on the location x_0 of the initial pulse. Figure 7 shows that the fundamental (harmonic) standing wave excitation time t_{ex} generally grows (declines) as the pulse position x_0 moves from the loop foot-point ($x_0 = 0$) to its apex ($x_0 = L/2$). In the case of the fundamental standing wave, the damping time depends weakly on x_0 with a slight tendency to decrease with x_0 (bottom panel of Fig. 7). The second standing wave damping time decreases as x_0 approaches $L/2$.

These results support evidence that excitation and damping times are not constant but depend on the location of the initial pulse. Excitation time varies from its lowest value of $3\,T_1$ for $x_0 = 0$ to its highest value of $16\,T_1$ for $x_0 = 0.45\,L$ for the fundamental standing wave (and from $3\,T_2$ for $x_0 = L/2$ to $8\,T_2$ for $x_0 = 0.45\,L$ in the case of the second standing wave). The obtained values of damping time are in the

range $4.7\,T_1 < \tau < 5.2\,T_1$ for the fundamental standing wave and $5\,T_2 < \tau < 6.1\,T_2$ for the second standing wave, for which the lowest (highest) value is obtained for $x_0 = L/2$ (for $x_0 = 0.44\,L$). Note that $T_1 \approx 2T_2$, so that in absolute terms the 2nd wave is damped more rapidly than the fundamental wave.

We conclude from the above results that the fundamental (harmonic) standing wave is excited most efficiently by an initial pulse located in the neighborhood of a loop foot-point (of the loop apex). At these points the excitation (damping) time of these waves is equal to 3 (5) periods, corresponding roughly to 13 min (11 min).

The standing wave excitation time varies with density contrast d (Fig. 8). For high values of d the fundamental standing wave is excited less efficiently than for low values, for which t_{ex} attains its minimum; the excitation time is doubled. At the smallest (largest) considered value of $d = 10^2$ ($d = 10^8$) the damping time is $2.5\,T_1$ ($6.2\,T_1$). From these results we conclude that the fundamental standing wave is excited faster in low density contrast regions, as such a structure is more susceptible to energy leakage at the foot-points. As a consequence, it is easier for a perturbation to adjust to standing waves profiles. Obviously, damping of the wave is enhanced and the damping time is of the order of a few wave periods. Damping is about twice weaker at $d = 10^8$ than at $d = 10^2$, although the dependence of τ on d is complex.

The standing wave excitation time depends on pulse width w (Fig. 9). For a sufficiently wide pulse the fundamental standing wave is excited faster by wider pulses, although there is significant scatter (top panel). The damping time oscillates around a value of about $4.8\,T_1$, within a relatively narrow range implying that it is almost independent of w. These results are a consequence of the fact that wider pulses are closer to the sine
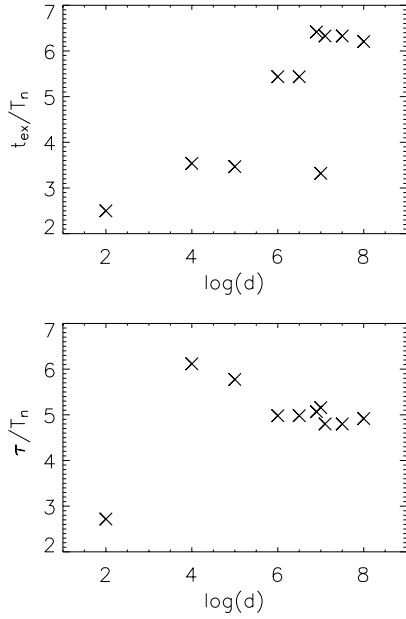
Fig. 8. Normalized fundamental standing wave excitation time (*top panel*) and normalized damping time (*bottom panel*) vs. $\log d$ for $w = L/40$ and $x_0 = L/4$.
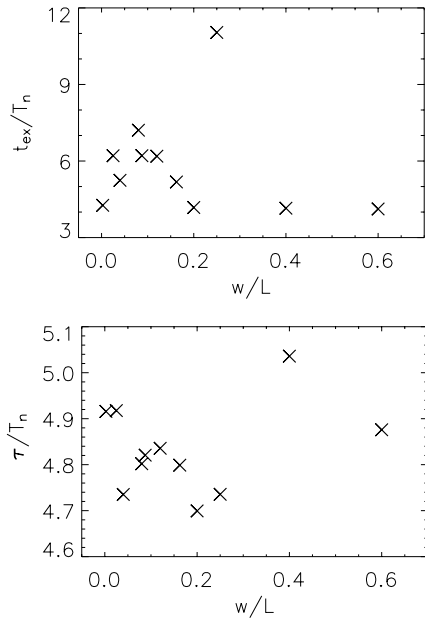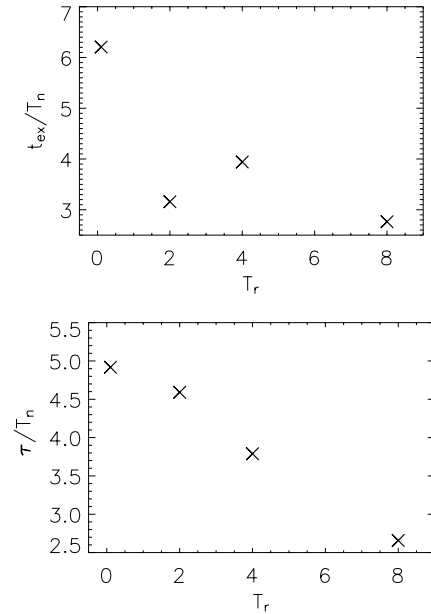

Fig. 9. Normalized fundamental standing wave ($n = 1$) excitation time t_{ex}/T_n (*top panel*), and damping time τ/T_n (*bottom panel*) vs. pulse width w for $d = 10^8$ and $x_0 = L/4$.

function of x of the standing wave spatial profile of Eqs. (13)–(15); sufficiently wide pulses adjust faster to the standing waves.

In the case of the second standing mode, its excitation and damping times vary with the pulse width (Table 1). For a very wide pulse the second standing wave is excited more slowly than by narrower pulses, but its damping time is slightly shorter. Note that, even for $w = 3 \times 10^9$ cm, the initial pulse is close to the sine function of x and the second, not the fundamental, mode is excited for pulse position $x_0 = L/2$.

Table 1. Excitation time t_{ex} and damping time τ for two different widths of the pulse in the case of the second ($n = 2$) standing wave for $d = 10^8$ and $x_0 = L/2$.
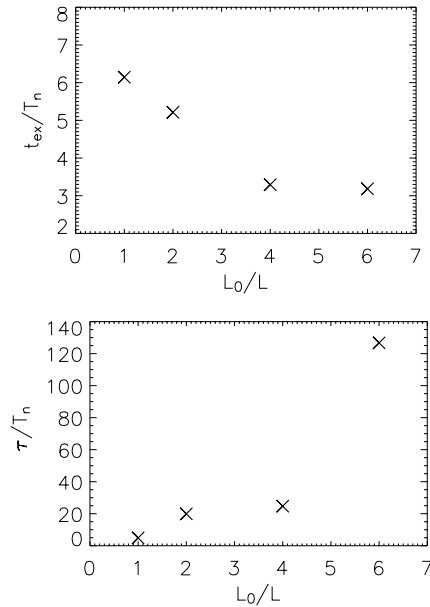
w/L	t_{ex} [s]	τ [s]
0.025	463	603
0.6	1050	565

Fig. 10. Normalized fundamental standing wave excitation time (*top panel*) and damping factor (*bottom panel*) vs. normalized pulse temperature T_r for $d = 10^8$, $w = L/40$, and $x_0 = L/4$.

So far, we have discussed the initial pulses of constant relative temperature $T_r = T_p/T_c = 1.1$, where T_p is the temperature of the initial pulse and T_c is the temperature of the corona. This temperature is realized through the choice of pulse amplitudes $A_\varrho = 0.125\varrho_0(x_0)$ and $A_p = 0.25p_0$. It is worth quantifying an influence of T_r on mode excitation time t_{ex} and damping time τ. To do so, we consider three values of the temperature ratio: $T_r = 2$ ($A_\varrho = 0.125\varrho_0(x_0)$, $A_p = 1.25p_0$), $T_r = 4$ ($A_\varrho = 0.125\varrho_0(x_0)$, $A_p = 3.5p_0$), $T_r = 8$ ($A_\varrho = 0.125\varrho_0(x_0)$, $A_p = 8.0p_0$). Figure 10 summarizes results of the corresponding numerical experiments. According to our expectation a warmer pulse leads to more efficient standing wave excitation as the excitation time declines with T_r; a warmer pulse transfers itself in a shorter time to a sinusoidal standing wave profile. As a consequence of higher energy leakage, the standing wave is more rapidly damped for higher values of T_r. Given that T_r changes by a factor of 8, the induced changes in t_{ex} and τ are relatively small (factor of 2). As warmer pulses correspond to higher amplitudes of the initial pulses we claim that nonlinearity does not play a vital role in affecting t_{ex} and τ.

We now compare four cases which correspond to the following loop lengths L_0: (a) $L_0 = L = 50 \times 10^8$ cm; (b) $L_0 = 2L$; (c) $L_0 = 4L$; and (d) $L_0 = 6L$. The pulse position was chosen as $x_0 = L_0/4$. The normalized excitation time decreases with the loop length for narrow pulses (Fig. 11), and the damping time generally grows with loop length L_0 (right panel). Note

Fig. 11. Normalized fundamental standing wave excitation time (*top panel*) and damping time (*bottom panel*) vs. normalized loop length L_0, for $d = 10^8$, $x_0 = L_0/4$, and $w = L/40$. Note that T_n now corresponds to the expected period for the appropriate loop length.

Fig. 12. Normalized fundamental standing wave excitation time (*left panel*) and damping time (*right panel*) vs. the velocity amplitude of the initial pulse, A_V, for $d = 10^8$, $w = L/40$, $x_0 = L/4$ (squares), and $x_0 = L/2$ (crosses).

that since $T_n \sim L_0$ the results must be considered carefully, e.g. t_{ex} actually grows with L_0 (in s).
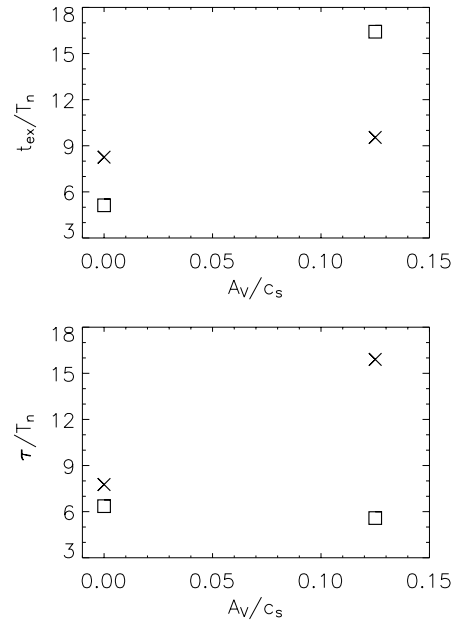
3.3. Velocity pulses

In a similar case to the cases discussed above, the only difference is that to mass density and pressure perturbations we add a non-zero pulse in velocity. We choose and hold fixed $A_V = 0.125 \, c_s(x_0)$. In the case of $x_0 = L/4$ the fundamental standing wave is generated at $t_{ex} \approx 7 \, T_1$, which is a little larger than in the case of $A_V = 0$ (Fig. 12). The damping time attains a value of $\tau \approx 5.5 \, T_1$, which is 10% higher than without the velocity pulse. From this result we conclude that the fundamental mode is weakly damped while triggered by the velocity perturbations.

In the case of both $x_0 = L/2$ and the harmonic standing wave (crosses) the excitation time is larger than in the case of $A_V = 0$, while the damping time becomes a bit smaller than without the velocity pulse. The harmonic standing wave is excited in a longer lapse of time and is stronger damped while being excited by a velocity pulse.

3.4. Perturbations of non-ideal plasma

Next we consider several cases of non-ideal plasma with different effects switched on. In our approach we neglect background heating, which has been used by Nakariakov et al. (2004) to keep background temperature at the coronal value of ~1 MK. Instead, we direct most of our attention to the effect of non-ideal plasma on wave propagation. Table 2 summarizes all the results that are obtained for the width of the pulse $W = L/40$ and its initial position $x_0 = L/4$.

We discuss in some detail the case of thermal conduction, heating, and cooling acting simultaneously. In this case we do not observe a pure standing wave but instead a packet of waves with largest contribution from the fundamental standing wave (left bottom panel of Fig. 13). Mass density collected at $x_d = L/4$ exhibits oscillations that decay in time. The mean value of the mass density grows in time as a result of thermal conduction (right top panel of Fig. 13). Velocity spectra reveal the mean period of $T_1 = 410$ s (bottom panels of Fig. 13). Note that this value is higher than in the case of the ideal plasma due to a different value of the effective sound speed $c_s^{eff} = \sqrt{\gamma p/\varrho}$ that results from the cooling and thermal conduction (Fig. 14).

It is noteworthy that thermal conduction acting alone excites a bunch of waves at the loop foot-points where the thermal conduction is mostly effective (not shown). The most significant value of standing wave period is similar to the case without conductivity. Taking both thermal conduction and heating into account leads to a significant increase in the period of the observed standing wave. In the case of thermal conduction switched on, evaporation of a photospheric plasma takes place. It is interesting, however, that it is not continuous but occurs in the form of parcels which propagate out of the photosphere in certain lapses of time with each separate from the other.

This scenario can be explained as follows. Photospheric plasma gets heated due to thermal conduction. As this heated material is denser than a coronal plasma, a sufficient amount of heating is needed for a parcel of the photospheric gas to attain enough pressure to leave the photosphere.

4. Summary

In this paper we have considered the excitation and damping of slow standing waves in a solar coronal loop that is

Table 2. Standing wave period T, excitation time t_{ex}, and damping time τ for various run parameters in cgs units. The sign $-$ means that a value could not be evaluated.
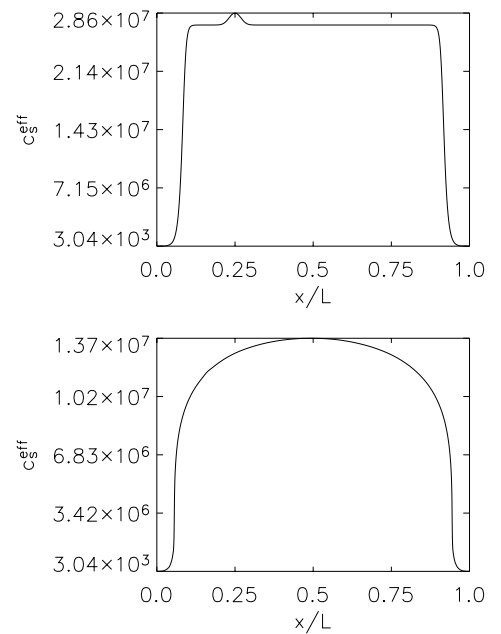
A_ϱ	A_p	A_V	d	$c_s[\text{cm s}^{-1}]$	$\mathcal{H}$	$\mathcal{L}$	σ	$T[\text{s}]$	$t_{ex}[\text{s}]$	$\tau[\text{s}]$
$\neq 0$	$\neq 0$	$=0$	10^8	0.35×10^8	$=0$	$=0$	$=0$	254	1578	1250
$\neq 0$	$\neq 0$	$=0$	10^8	0.35×10^8	$\neq 0$	$=0$	$=0$	208	915	986
$\neq 0$	$\neq 0$	$=0$	10^8	0.35×10^8	$\neq 0$	$\neq 0$	$=0$	208	916	998
$=0$	$=0$	$=0$	10^8	0.35×10^8	$\neq 0$	$\neq 0$	$=0$	208	919	1009
$=0$	$=0$	$=0$	10^8	0.35×10^8	$=0$	$=0$	$\neq 0$	$-$	$-$	$-$
$\neq 0$	$\neq 0$	$=0$	10^8	0.35×10^8	$=0$	$=0$	$\neq 0$	500	1291	2289
$\neq 0$	$\neq 0$	$=0$	10^8	0.35×10^8	$\neq 0$	$=0$	$\neq 0$	556	1133	1178
$=0$	$=0$	$=0$	10^4	0.35×10^8	$=0$	$=0$	$\neq 0$	278	$-$	$-$
$\neq 0$	$\neq 0$	$=0$	10^4	0.35×10^8	$=0$	$=0$	$\neq 0$	455	$-$	$-$
$\neq 0$	$\neq 0$	$=0$	10^8	0.1×10^8	$=0$	$=0$	$=0$	882	4627	3826
$\neq 0$	$\neq 0$	$=0$	10^8	0.1×10^8	$=0$	$=0$	$\neq 0$	909	1113	3930
$\neq 0$	$\neq 0$	$=0$	10^8	0.35×10^8	$\neq 0$	$\neq 0$	$\neq 0$	400	827	2170
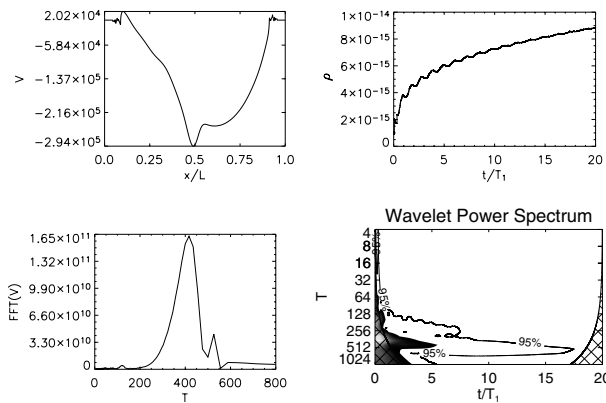
Fig. 13. A spatial velocity profile at $t \approx 12\, T_1$ (*left top panel*), the corresponding time-characteristics of mass density signal (*right top panel*), the Fourier spectrum (*left bottom panel*), and the wavelet spectrum (*right bottom panel*) for $d = 10^8$, $w = L/40$, $x_0 = L/4$, $\sigma \neq 0$, $\mathcal{H} \neq 0$, $\mathcal{L} \neq 0$, $A_\varrho \neq 0$, $A_p \neq 0$, and $A_V = 0$.

Fig. 14. Effective sound speed at $t = 0$ (*top panel*) and $t = 5000$ s (*bottom panel*) in the case of Fig. 13.

approximated by a one-dimensional plasma. Our model implements optionally thermal conduction, heating, cooling, and impulses in plasma quantities. The thermal conductivity follows the formulation of Spitzer (1962). The phenomenological heating source term is localized in space and time. Cooling is due to radiative losses from an optically thin plasma. A Fast Fourier transform and wavelet analysis of temporal wave profiles have shown that in a loop the fundamental or harmonic standing slow waves are excited depending on the location of the trigger. We worked out a simple criterion for the presence of a standing wave based on a phase shift between perturbed mass density $\delta\varrho$ and velocity V. The time required for a standing wave to settle in a loop from a hot initial pulse is of the order of a dozen or so wave periods and varies, depending on such parameters of the plasma as the initial location of the pulse, the density contrast, or the pulse width. In the case of a wide and strong pulse, as well as of heated plasma, this time-scale is shorter.

The one-dimensional model we have developed obviously suffers from several drawbacks. Its main shortcoming is that it only takes slow magnetosonic waves into account and neglects the presence of fast and Alfvén waves in the system. As a consequence, this model excludes several likely damping mechanisms that were already suggested in the literature. However, these neglected effects are believed to be unimportant as far as the scenario of slow wave excitation and damping are concerned. More realistic models of slow wave development are currently under development and the results will be reported elsewhere.

References

Aschwanden, M., Fletcher, L., Schrijver, C., & Alexander, D. 1999, ApJ, 520, 880

Curdt, W., Wang, T. J., Dammasch, T. E., & Solanki, S. K. 2003, Hvar Obs. Bull., 27, 83

De Moortel, I., & Hood, A. W. 2003, A&A, 408, 755

De Moortel, I., Hood, A. W., & Ireland, J. 2002a, A&A, 381, 311

De Moortel, T., Hood, A. W., Ireland, J., & Walsh, R. W. 2002b, Sol. Phys., 209, 89

Fryxell, B., Olson, K., Ricker, P., et al. 2000, ApJS, 131, 273

Nakariakov, V. M., Ofman, L., DeLuca, E. E., Roberts, B., & Davila, J. M. 1999, Science, 285, 862

Nakariakov, V. M., Verwichte, E., Berghmans, D., & Robbrecht, E. 2000, A&A, 362, 1151

Nakariakov, V. M., Tsiklauri, D., Kelly, A., Arber, T. D., & Aschwanden, M. J. 2004, A&A, 414, L25

Ofman, L. 2002, ApJ, 568, L135

Ofman, L., & Wang, T. J. 2002, ApJ, 580, L85

Ofman, L., & Aschwanden, M. 2002, ApJ, 576, L153

Ofman, L., Nakariakov, V. M., & Sehgal, N. 2000, ApJ, 533, 1071

Roberts, B. 2000, Sol. Phys., 193, 139

Ruderman, M. S., & Roberts, B. 2002, ApJ, 577, 475

Spitzer, L. 1962, Physics of fully ionized gases (New York: Wiley)

Torrence, C., & Compo, G. P. 1998, Bull. Amer. Meteor. Soc., 79, 61

Tsiklauri, D., Nakariakov, V. M., Arber, T. D., & Aschwanden, M. J. 2004, A&A, 422, 351

Van Doorsselaere, T., Debosscher, A., Andries, J., & Poedts, S. 2004, A&A, 424, 1065

Wang, T. J., Solanki, S. K., Curdt, W., Innes, D. E., & Dammasch, I. E. 2002, ApJ, 574, L101

Wang, T. J., Solanki, S. K., Innes, D. E., Curdt, W., & Marsch, E. 2003a, A&A, 402, L17

Wang, T. J., Solanki, S. K., Curdt, W., et al. 2003b, A&A, 406, 1105

Zingale, M., Dursi, L. J., ZuHone, J., et al. 2002, ApJS, 143, 539